

Exploratory Study for Computation/Measurement of Underwater Ship Radiated Noise toward Marine Environmental Protection

by

Hikaru KAMIIRISA*, Nobuaki SAKAMOTO** and Akiko SAKURADA***

Abstract

Underwater ship radiated noise (USRN) has been a large interest among maritime industries in terms of mariners' comfort as well as environmental protection. This is evidenced by the fact that International Maritime Organization and several European Union (EU) projects have released non-mandatory guidelines for the reduction of underwater noise from commercial shipping to address adverse impacts on marine life. Japan is also ought to deal with this issue. In this study exploratory investigations are carried out for estimations in USRN, specifically for propeller cavitation noise by means of viscous computational fluid dynamics (CFD) and full scale field measurement. In the former investigation, two methodologies have been tested to predict frequencies and sound pressure level (*SPL*) of noise originated from propeller cavitation, i.e. 1) direct estimation of *SPL* using pressure signal from CFD simulation, and 2) indirect estimation of *SPL* using semi-empirical formula with CFD simulation. The results are encouraging in that the present CFD simulation is capable of capturing sheet cavitation and resultant tonal noise. The estimation of broadband noise is still challenging by the present CFD simulation yet its application in conjunction with the semi-empirical formula is likely to be effective for predicting its upper bound. In the latter investigation, full scale field experiment is carried out to measure source level of propeller cavitation noise emitted from an inland liner operating at domestic remote islands. The measurements are based on the guideline by International Standard Organization. The differences of *SPL* in tonal noise depending on broadside and engine load are successfully captured, and the validity of the present measurement methods in full scale is confirmed. The experimental data would be quite useful for future validation in computational results. In addition to the computational and experimental investigations, state-of-art outcomes from three EU projects relevant to USRN are reviewed in order to earn useful information for on-going domestic projects.

* 流体設計系, ** 流体設計系 流体制御研究 Gr., *** 流体設計系 実海域性能研究 Gr.

原稿受付 平成28年5月26日

審査日 平成28年6月20日

Table of Contents

1. Introduction	66
2. Prediction of near field cavitation noise by CFD	67
2.1 Background and motivation	67
2.2 Computational method	67
2.2.1 Flow field	67
2.2.2 Sound pressure level	67
2.3 Simulation design	68
2.3.1 Geometry and flow condition	68
2.3.2 Computational setup	69
2.3.3 Validation data and variables	70
2.4 Results	70
2.4.1 Cavitation extent in the ship wake	70
2.4.2 Propeller cavitation noise	73
2.5 Summary	74
3. Field measurement of underwater ship radiated noise	74
3.1 Measurement condition	74
3.2 Measurement of water temperature and salinity	75
3.3 Measurement of underwater ship radiated noise	76
3.3.1 Measurement method	76
3.3.2 Measurement device	77
3.3.3 Analysis method	78
3.3.4 Results	78
4. Review of relevant EU projects	80
4.1 Three EU projects related to ship radiated noise	80
4.2 Some representative results from SILENV, AQUO and SONIC	81
4.2.1 SILENV	81
4.2.2 AQUO	82
4.2.3 SONIC	85
5. Concluding remarks	85
Acknowledgements	86
Reference	86

1. Introduction

Underwater ship radiated noise (USRN) has been a large interest among maritime industries in terms of mariners' comfort as well as environmental protection. In 1995, International Council for the Exploration of the Sea (ICES) released the guidelines of underwater ship radiated noise for fishery research vessels¹⁾. In 2014, International Maritime Organization (IMO) released the guidelines for the reduction of underwater noise from commercial shipping to address adverse impacts on marine life²⁾. The former directly regulates the upper limit of radiated sound pressure level (*SPL*) while the latter regulates the 1st and 2nd blade rate harmonic amplitudes of stern pressure fluctuation depending on the bluntness (e.g. block coefficient C_B) of the ship. European Union (EU) countries organized three research projects, e.g. "SILENV"³⁾, "AQUO"⁴⁾ and "SONIC"⁵⁾, to investigate experimental and computational methods for assessing environmental impact of underwater ship radiated noise. The regulations from ICES and IMO are still non-mandatory, yet they COULD BE mandatory in the future. Japan must be

prepared for such scenario. In 2015, the domestic project “Research study on the effect of underwater ship radiated noise to marine fauna” has been organized by Japan Ship Technology Research Association (JSTRA) as the first step for the preparation. National Maritime Research Institute (NMRI) is a core member of this project and the task is to investigate computational and measurement methods for the source level of underwater ship radiated noise. Two major components of underwater ship radiated noise are 1) low frequency and periodic machinery noise which is originated from main and auxiliary engines, and 2) high frequency/broadband flow noise which is originated from marine propulsors. Although the former is important, the latter is the most dominant noise source under the normal navigation speed and thus is of interest in the present study.

Followed by this introduction, Chapter 2 presents the computational estimation of near field propeller cavitation noise, Chapter 3 describes the field measurement of USRN carried out at coastal area of Japan, Chapter 4 provides brief overviews of state-of-art EU projects, and Chapter 5 summarizes the conclusion and the future plans.

2. Prediction of near field cavitation noise by CFD

2.1 Background and motivation

Numerical estimation of propeller cavitation and resultant noise are usually challenging since the flow field around cavitating propeller contains multiscale flow physics, i.e. phase change of the fluid, turbulence, unsteady loading on the propeller blade etc. This is the reason why the propeller cavitation noise has both tonal and broadband frequencies. To capture such noise characteristics, local pressure fluctuation needs to be predicted accurately in both near field and far field of noise source. Modeling dynamics of cavitation bubble by nonlinear Rayleigh-Plesset equation contributes to estimate pressure fluctuation with high frequency and resultant broadband noise⁶⁾. Yet this method requires assumptions in volumetric change of cavitation bubble in time as well as distribution of bubble radius. The empirical formula based on full scale measurement⁷⁾ is able to provide rough estimation in the upper bound of *SPL*. Although this method is practical, full scale measurement is expensive in cost and time. Viscous computational fluid dynamics (CFD) can be an alternative to compensate the disadvantages of former two methods. Unsteady propeller cavitation is solved by Reynolds-averaged Navier Stokes (RaNS) equation together with an appropriate cavitation model. The solution can directly be utilized for noise estimation in near field. Yet the capability of viscous CFD for propeller cavitation noise is still unknown. Cavitation model is usually based on simplified Rayleigh-Plesset equation with mixture, single-fluid model thus there may be limitations to capture growth and collapse of cavitation bubble. The pressure fluctuation may numerically be diminished due to diffusion arose from spacial and temporal discretizations. The aim of the present study is to understand the capability of viscous CFD in estimating propeller cavitation noise in the near field.

2.2 Computational method

2.2.1 Flow field

The computational results are obtained using general-purpose commercial CFD package STAR-CCM+ ver10.06.009 (double precision version)⁸⁾. The governing equations are the continuity and unsteady RaNS equations with dimensional forms, and are solved by finite volume method. Rotational motion of a propeller is modeled by dynamic overset technique. Among several turbulence models on the solver, *k- ω SST* based Detached Eddy Simulation (DES) is selected based on the past studies. The boundary layer is assumed being “fully developed”, in other words, no transition model has been introduced. The turbulent boundary layer is fully resolved without wall function. As the two-phase flow modeling, Volume of Fluid (VoF) method is utilized in conjunction with the cavitation model by Schnerr and Sauer (2001)⁹⁾. Divergence free condition is satisfied by solving pressure Poisson equation iteratively using Semi-Implicit Method for Pressure-Linked Equation (SIMPLE)-type algorithm. The order of accuracy is second in both space and time. The code is parallelized by Message Passing Interface (MPI) and is ran on distributed memory type machines with 116 CPUs.

2.2.2 Sound pressure level

Two methods are tested in the present study to estimate *SPL* originated from cavitating propeller. First method is to utilize time history of pressure sampled at certain hydrophone location directly from the CFD simulation. The data is subjected to Fast Fourier Transform (FFT) with Hanning window, and then filtered by 1/3 octave band. The amplitude of the signal are integrated within the lower and upper frequency over each band width, and converted into *SPL* relative to $1\mu\text{Pa}$ as

$$G = \left| \int_{-\infty}^{\infty} p(t) \exp(-j2\pi ft) dt \right|^2 \quad (2.1)$$

$$SPL = \int_{f_c - \Delta f_c / 2}^{f_c + \Delta f_c / 2} G(f) df$$

where G is the power spectral density per 1Hz, $p(t)$ is the time history of the pressure at certain receiver location, f_c is the central frequency of 1/3 octave band¹⁰⁾. Second method is to utilize Brown's formula⁷⁾ together with the CFD simulations. It is presented as

$$SPL = K + 10 \log(BD_p^4 n^3 f^{-2}) + 10 \log(A_c / A_D) \quad (2.2)$$

where *SPL* [*dB rel* $1\mu\text{Pa} / \sqrt{\text{Hz}}$ at 1m] is the sound pressure level, $K(=163)$ is an empirical constant, B is the number of blades, D_p [m] is the propeller diameter, n [rps] is propeller rotation speed, f [Hz] is the target frequency, $A_c[\text{m}^2]$ is the area of cavitation extent on the blade, and $A_D[\text{m}^2]$ is the area of the blade. The CFD simulation estimates A_c/A_D and the results are plugged into Eq. (2.2) to estimate *SPL* for certain f .

2.3 Simulation design

2.3.1 Geometry and flow condition

The conventional propeller (CP) and highly-skewed propeller (HSP2) which used to be equipped on the training ship "Seiun 1st" are of the interest in the present study¹¹⁾. The CP was initially equipped on the ship, and then the HSP2 was retro-fitted subsequent to the CP aiming to reduce hull vibration. Table 2.1 summarizes major dimension of these propellers together with their overview in Fig. 2.1. In order to represent flow condition, three non-dimensional parameters are introduced as

$$Rnk = \frac{c_{0.7R} \sqrt{V_a^2 + (0.7\pi n D_p)^2}}{\nu} \quad (2.3)$$

$$\sigma_n = \frac{P_A + \rho g(I - h) - P_v}{0.5\rho(nD_p)^2} \quad (2.4)$$

$$K_T = \frac{T}{\rho n^2 D_p^4} \quad (2.5)$$

where Rnk is Kempf's Reynolds number, $c_{0.7R}$ [m] is the chord length of the blade section at 70% of propeller radius R , V_a [m/s] is the advance velocity, ν [m²/s] is the dynamic viscosity, σ_n is the cavitation number, P_A [Pa] is the atmospheric pressure, ρ [kg/m³] is the fluid density, g [m/s²] is the gravitational acceleration, I [m] is the immersion depth of the propeller shaft, h [m] the reference height, P_v [Pa] is the vapor pressure, K_T is the thrust coefficient and T [N] is the propeller thrust. In the present study, following parameters are set in such a way that the computational flow conditions follow the experiments¹²⁾¹³⁾; $Rnk \sim 6.5E+05$ and $n=20.0$ [rps] for all the cases, $(K_T, \sigma_n)=(0.207, 3.06)$ for CP and $(0.201, 2.99)$ for HSP2, respectively. Two parameters are set to quantify the property of nuclei for cavitation modeling, e.g. 1) density of the nuclei is set to $1.0E+14$ [1/m³], and 2) radius of the nuclei is set to 1.0 [μm], which are the same as utilized by Bijlard (2014)¹⁴⁾.

Table 2.1 Major dimension of model propellers

Propeller	CP(MPNO. 218)	HSP2(MPNO. 220)
D_p (m)	0.221	0.220
Pitch ratio at $r/R=0.7$	0.950	0.944
E.A.R.	0.650	0.700
Boss ratio	0.197	
Number of blades	5	
Skew (deg.)	10.50	45.00
Rake (deg.)	6.00	-3.03
Wing section	MAU	Mod. SRI-B

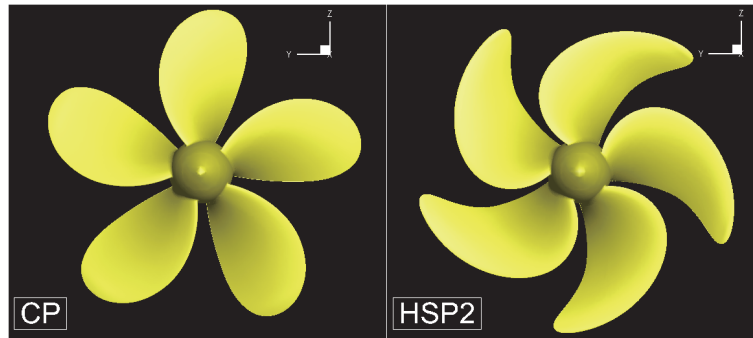


Figure 2.1 Overview of the propellers

2.3.2 Computational setup

The coordinate system is right-handed Cartesian, and its center is coincident with the boss center of a propeller. The flow direction is x negative to x positive, and the propeller rotates clockwise around x-axis observing from downstream. Figure 2.2 presents the computational grid. Trimmed-cell is utilized for grid generation, and nondimensional viscous length y^+ is close to 1 in order to meet the requirement for the present turbulence model. It consists of two cylindrical volume parts, e.g. stator for which the computational domain remains stationary during the simulation and rotator for which the computational domain rotates together with the propeller motion, and necessary local refinements placed at $r/R \sim 0.5$ toward the tip to resolve sheet and tip vortex cavitation. The propeller is placed inside the rotator, and the flow variables between stator and rotator are exchanged via dynamic overset approach. As an overset assemble process, cells in each region are flagged as 1) donor, 2) receptor, 3) active, and 4) inactive. Figures 2.2(a) and 2.2(b) show the flags which present the status of overset cells in stator and rotator, respectively. The cells colored by light-green are “active” cells where governing equations are solved. The cells colored by red are “inactive” cells where governing equations are not solved. The cells colored by blue are “receptor”. The donor cells around the receptor are searched using linear scheme with shape function of spanning tetrahedron which means that one receptor has 4 donor stencils. The donor cells in stator provide flux variables to receptor cells in rotator and vice versa. The flux variables ϕ are interpolated from donor cells to a receptor cell as

$$\phi_{receptor} = \sum_i \alpha_i \phi_{i,donor} \quad (2.6)$$

where i is the cell ID and α_i is the interpolation coefficients for flux variables of donor cell i . Total number of cells is approximately 19M. Followed by Hasuike et al. (2010)¹⁵⁾'s investigation, the distance from the coordinate center to the inflow boundary, far-field boundary and outflow boundary are $0.7D_p$, $5D_p$ and $5D_p$, respectively. Physical time advancement is set in such a way that the propeller rotates 1deg per time step with 20 sub iterations.

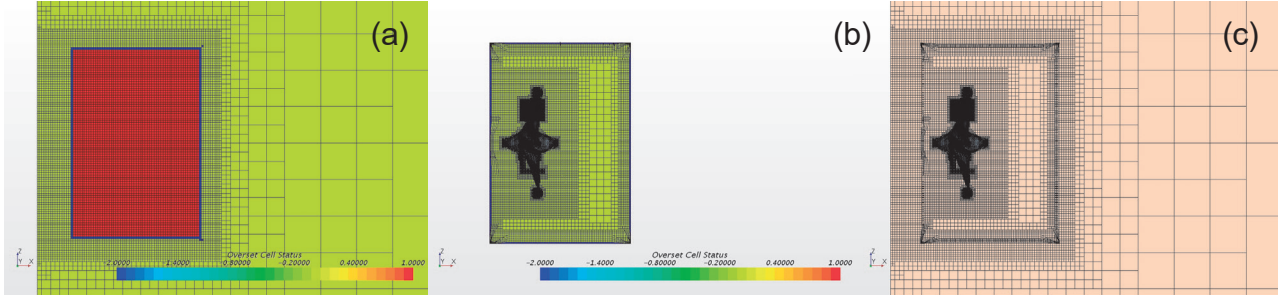


Figure 2.2 Overset grid assembly: (a) stator, (b) rotator, (c) assembled grid

2.3.3 Validation data and variables

Cavitation pattern is quantified by the time histories of the area of cavitation extent A_c [mm²] on the key blade, and the volume of cavitation bubble V_c [mm³] in the rotator domain. The measurement of these quantities were carried out by Kudo et al. (1989)¹³ by a laser beam coupled with Charge Coupled Device (CCD). To compute A_c and V_c from the present CFD results, the following criteria are utilized;

$$A_c|_{CFD}(t) \cong \sum_{i=1}^{N_f} s_i \beta_i(t) \text{ where } \beta_i(t) = \begin{cases} 1 & \text{if } \alpha_i(t) \geq 0.1 \\ 0 & \text{otherwise} \end{cases} \quad (2.7)$$

$$V_c|_{CFD}(t) \cong \sum_{i=1}^{N_c} v_i \alpha_i(t) \text{ where } \alpha_i(t) = \begin{cases} \alpha_i(t) & \text{if } \alpha_i(t) \geq 0.1 \\ 0 & \text{otherwise} \end{cases}$$

where N_f is the number of faces on the key blade, s_i [mm²] is the area of discretized faces, $\beta_i(t)$ is the flag to determine the area of cavitation extent on the key blade, $\alpha_i(t)$ is the instantaneous volume fraction of gas phase, N_c is the number of cells in the rotator domain, and v_i [mm³] is the volume of discretized cells.

For the *SPL*, the model scale data was measured at small-sized cavitation tunnel with ship wake generated by wire-mesh screen while the full scale measurement was carried out using two hydrophones placed in the vicinity of propeller tip¹¹. Figures 2.3(a) and 2.3(b) show the configurations of model and full scale experiments, respectively, for which the hydrophone positions are geometrically similar between the two.

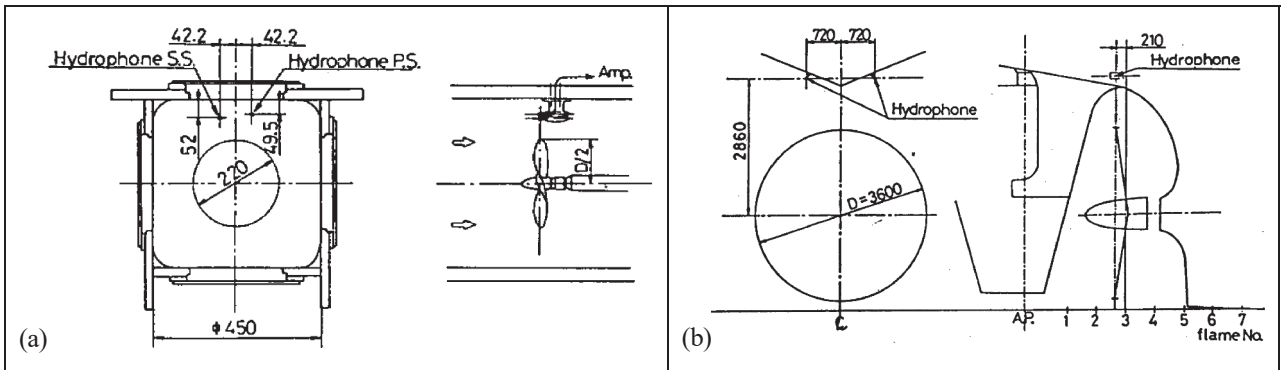


Figure 2.3 Hydrophone arrangement¹¹: (a) model experiment, (b) full scale sea trial

2.4 Results

2.4.1 Cavitation extent in the ship wake

Figure 2.4 describes the distribution of axial velocity imposed on the inflow boundary. Radial and tangential components are set to zero. To obtain this flow pattern, wake survey was carried out at towing tank, and then the extrapolation method proposed by Sasajima&Tanaka was applied in order to take scale effect into consideration¹¹.

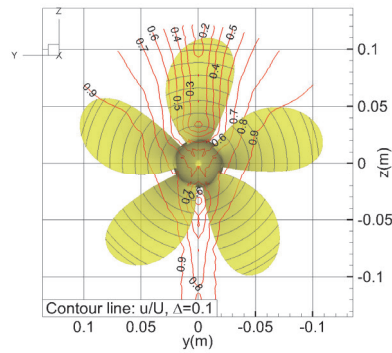


Figure 2.4 Full scale ship wake imposed at inflow boundary

Cavitation pattern: Figures 2.5 and 2.6 summarize the experimental¹²⁾ and computational results of cavitation pattern at different blade position θ for CP and HSP2, respectively. The cavitation bubble is depicted by volume fraction $\alpha=0.1$ iso surface. The computational results of sheet cavitation show nice agreement to the experimental data for both CP and HSP2. The tip vortex cavitation (TVC) is reproduced for the CP to some extent while it is not for the HSP2. As one of the design changes from CP to HSP2, decreased pitch distribution with large skew angle was introduced and thus HSP2 is tip-unloaded than CP. This attenuated the strength of tip vortex. In the present computation the spacial resolution is the same between CP and HSP2 which indicates that the spacial resolution to capture TVC utilized for CP is not enough for HSP2 and further spacially refined computations are necessary.

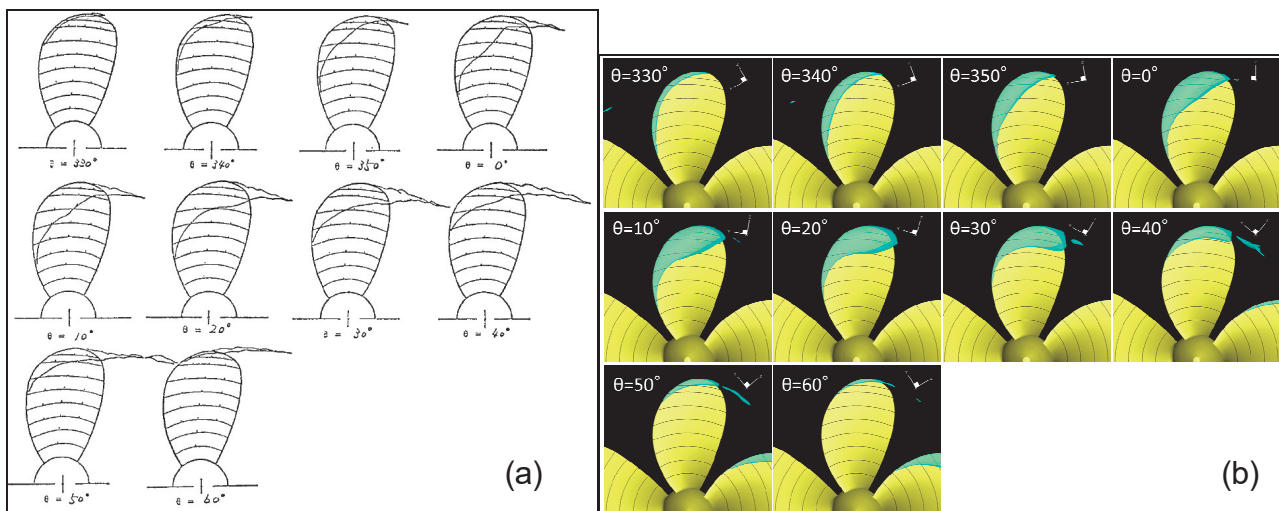


Figure 2.5 Cavitation pattern for CP: a) experiment¹²⁾, b) computation ($\alpha=0.1$)

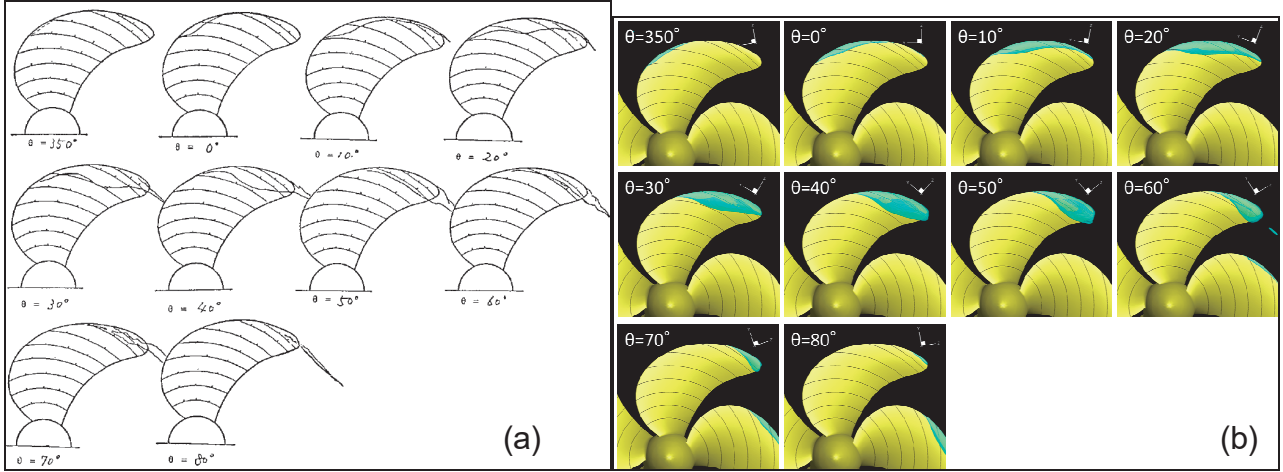


Figure 2.6 Cavitation pattern for HSP2: a) experiment¹²⁾, b) computation ($\alpha=0.1$)

Quantification of cavitation extent in time: Figures 2.7(a) and 2.7(b) present the time histories of A_c on the key blade and V_c over the rotor domain, respectively, as a function θ . The experimental¹³⁾ and reference computational results¹⁶⁾ of the A_c and V_c are put in Figs. 2.7a and 2.7b, respectively. Figure 2.8 compares the time history of nondimensional pressure $K_p(=p/(\rho n^2 D_p^2))$ logged at port and starboard hydrophone locations to that of the second derivative of V_c (termed d^2V_c/dt^2) calculated by 5-points central differencing scheme in the present computation and the referenced experiment. It is considered to be influential on pressure fluctuation since the pressure fluctuation due to volumetric variation of single spherical bubble is given by

$$\Delta p = \frac{\rho}{4\pi r} \frac{\partial^2 V_b(t-r/c)}{\partial t^2} \quad (2.8)$$

where r is the distance between bubble and arbitral field point, t is the time, c is the sound velocity, $V_b(=4/3\pi R_b^3)$ is the volume of single spherical bubble and R_b is the bubble radius¹⁷⁾. Table 2.2 summarizes the computational and the experimental results of maximum values of A_c/A_D and d^2V_c/dt^2 .

The computational results of A_c and V_c presented in Figs. 2.7(a) and 2.7(b) show quantitative difference to the experimental data. In the experiment the A_c remains almost constant at $-10\text{deg}<\theta<0\text{deg}$ (CP) and $20\text{deg}<\theta<40\text{deg}$ (HSP2) while the V_c is not constant in these range. It means that the thickness of cavitation bubble changes toward the blade normal direction at back side while the extent of sheet cavitation does not spread. The maximum values of the A_c and V_c are achieved at the same time when θ is 10deg (CP) and 30deg (HSP2). At $10\text{deg}<\theta<30\text{deg}$ (CP) and $40\text{deg}<\theta<50\text{deg}$, the A_c and V_c decrease at the same time, and they finally become similar level to those of -10deg (CP) and 0deg (HSP2) at $\theta=30\text{deg}$ (CP) and 50deg (HSP2). In the computational results, the A_c and V_c grow up in parallel. It means that the growth of the extent of sheet cavitation on the blade yields the increase of V_c for which it is consecutive to the cavitation pattern shown in Figs. 2.5 and 2.6. The A_c and V_c decrease at the same time for the CP while there is a phase difference between the two for the HSP2. Their rate of change in time is much smaller than those of the experimental data. The present computational results of A_c/A_D agree well with the reference computational results rather than the experimental data. The computational results of d^2V_c/dt^2 are at most 3.6 times smaller than that of the experimental data which indicates that the pressure fluctuation due to volumetric change of cavitation bubble may be less sensitive in the computational results than that of the experimental results. In Fig. 2.8 the time history of d^2V_c/dt^2 is almost in-phase with the time history of K_p for both CP and HSP2. It is interesting that the fluctuation of K_p with higher order blade frequencies (BF) are also well reproduced by d^2V_c/dt^2 . It indicates that an accurate estimation in V_c may contribute to indirect evaluation of pressure fluctuation with higher BFs.

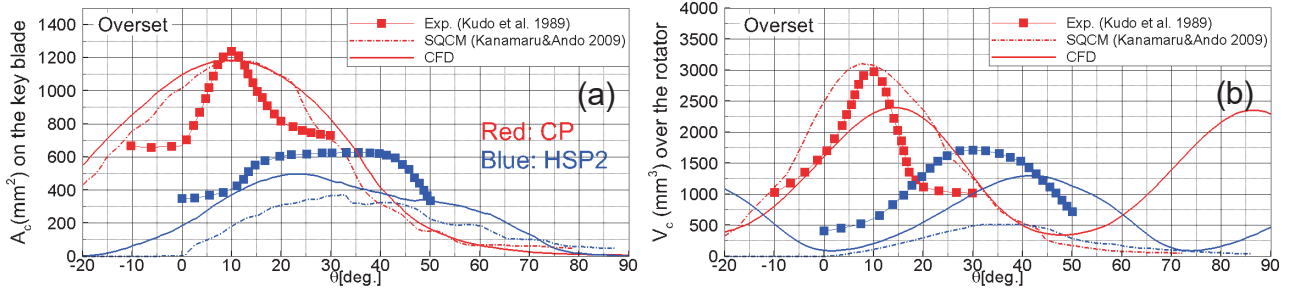


Figure 2.7 Quantification of cavitation extent in time:
 (a) extent area on the key blade, (b) volume of cavitation bubble in the computational domain

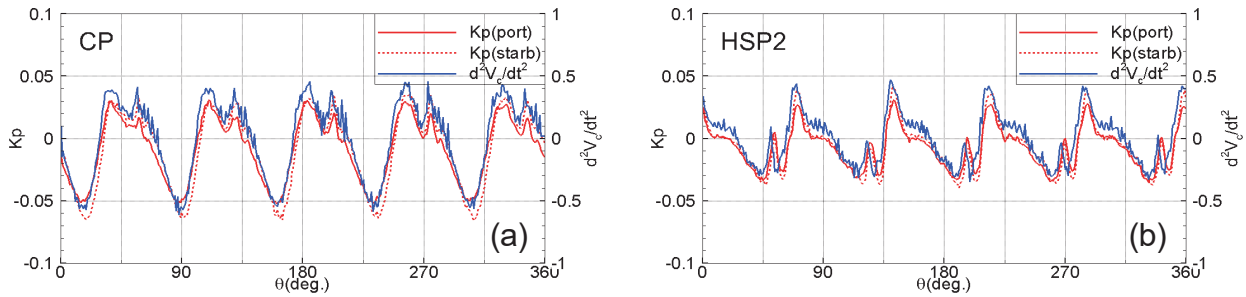


Figure 2.8 Comparison of time history between K_p and d^2V_c/dt^2 : (a) CP, (b) HSP2

Table 2.2 Maximum value of A_c/A_D and d^2V_c/dt^2

		$A_c/A_D[-]$	$\theta[deg.]$	$d^2V_c/dt^2[m^3/s^2]$	$\theta[deg.]$
CP*	Exp.	0.251	10	-2.01	10
	SQCM	0.239	12	-1.11	7.5
	CFD	0.238	10	-0.56	14
HSP2*	Exp.	0.114	35	-0.33	30
	SQCM	0.067	32	-0.62	40
	CFD	0.090	22	-0.30	42

2.4.2 Propeller cavitation noise

Figures 2.9 present the experimental and computational results of SPL evaluated at the port side hydrophone for CP and HSP2 in model and full scale. In order to consider scale effect in the computational results of model scale, Levkovskii's method is utilized¹¹⁾ as

$$\left. \begin{aligned}
 \lambda &= D_{ps} / D_{pm} \\
 \frac{f_s}{f_m} &= 1/\lambda \cdot (\sigma_{ns} / \sigma_{nm})^{0.5} \cdot V_s / V_m \\
 SPL_s - SPL_m &= 20 \log_{10} \left[\lambda^{1.5} \cdot (\sigma_{ns} / \sigma_{nm})^{0.5} \cdot V_s / V_m \cdot r_m / r_s \right]
 \end{aligned} \right\} \quad (2.9)$$

where the subscripts of “m” and “s” denote model and full scale, respectively, and $V_{s,m} = n_{s,m} D_{ps,pm}$. In the present study, σ_n is identical between model experiment and full scale measurement¹¹⁾ and thus $\sigma_{ns}/\sigma_{nm}=1$. The receiver position from the noise source is geometrically similar between model and full scale and thus $r_m/r_s=1/\lambda$. n_s is set to 163rpm.

Regardless to the difference in d^2V_c/dt^2 between the computational and experimental results, the computational result in model scale is able to capture tonal noise up to 2nd BF in CP and 7th BF in HSP2, respectively, compared to the experimental data. The broadband noise obtained by CFD is underestimated by 10dB compared to the experiment which is most probably due to the limitation of the present cavitation model, i.e. bubble growth and collapse cannot be well resolved. The full scale measurement shows that tonal noise due to 1st and 2nd BFs from HSP2 is 10dB smaller than that of CP due to decreased pitch distribution with higher skew angle. It contributes to decrease A_c and V_c which results in the decrease of pressure fluctuation with 1st BF approximately 1/3 of CP. The present CFD is likely to capture these phenomena, in the mean time, Levkovskii's scaling functions well. Therefore the computational result is able to reproduce the decrease of tonal noise due to 1st and 2nd BFs in HSP2 compared to CP. The Brown's formula successfully estimates upper bound of the SPL due to propeller cavitation. As shown in Table 2.2 and Fig. 2.9(c), the difference in A_c/A_D in CP and HSP2 is 5%Exp. and 21%Exp., respectively, which yields the difference in SPL less than 1dB for CP and approximately 1.2dB for HSP2, respectively.

2.5 Summary

Unsteady viscous CFD simulations are carried out for a cavitating marine propellers operating behind the ship wake. The computational results are consecutive in terms of cavitation pattern, time histories of the A_c and V_c and SPL . Especially for the A_c and V_c , detail diagnostics would be necessary in both experimental and computational results, e.g. the measurement criteria for the A_c and V_c as well as the thickness of the cavitation bubble along the blade. For the propeller cavitation noise, tonal and broadband noise are well predicted by the present computations up to certain frequencies in both model and full scale. In consequence, the present CFD, the Brown's formula and the Levkovskii's method are likely to be encouraging methods to estimate near field USRN due to propeller cavitation.

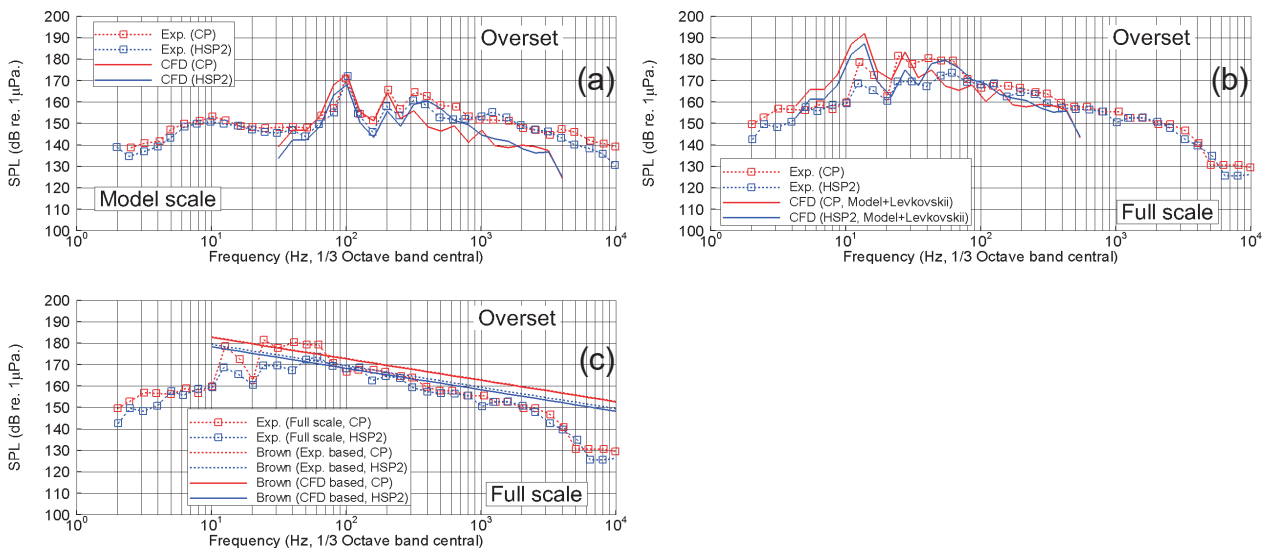


Figure 2.9 Experimental and computational results of near field SPL at port side hydrophone: (a) model scale, (b) full scale estimated by Levkovskii's method, (c) full scale estimated by Brown's formula

3. Field measurement of underwater ship radiated noise

Full scale field measurement of USRN was carried out for an inland liner. In this chapter, the details of the measurement, the analysis method and the result of the measurement are described.

3.1 Measurement condition

The measurement condition is shown below.

- Date : February 1st, 2016 9:00-15:00
 - Measurement area : Nishiizu Off Ugusu ; Water depth : more than 300m
 - Weather : Cloudiness
 - Wave, visual measurement : Significant wave : abt. 0.4m, Wave direction: North East
 - Wind, anemometer : Wind speed : abt. 2m, Wind direction: North East
 - Target ship : L_{PP} : abt. 50m, B : abt. 9m, d_d : 3.4m (stern trim : 0.6m)
 - Draught at the measurement : d_f : 2.3m, d_a : 3.6m
- Where L_{PP} is the length between perpendiculars, B is the ship breadth, d_d is the summer draught, d_f is the fore draught and d_a is the aft draught. The target ship is shown in Fig. 3.1.



Figure 3.1 Target ship

3.2 Measurement of water temperature and salinity

Water temperature and salinity play important roles in the sound propagation from the sound source to the hydrophone. Therefore the measurements are carried out for their vertical distribution from the free surface to the seabed. The measurement devices for water temperature and salinity are Expandable Bathythermograph (XBT) and Expandable Conductivity Temperature Depth profile (XCTD), respectively. These devices (probes) are set at the broadside. The specifications of these probes are summarized in Table 3.1. During the measurement, the target ship is at the rest to prevent the probes or the cable from being rolled up by the propeller. The measured results are shown in Fig. 3.2 and Fig. 3.3 in which T is the water temperature, h is the water depth from the water surface, and S is the salinity. In Fig.3.3, the salinity is 0 at about 592m which indicates the probe reaches to the seabed.

Table 3.1 Probe specifications

	Temperature			Electronic conductivity		
	Range	Accuracy	Resolution	Range	Accuracy	Resolution
XBT	-2~ 35°C	±0.2°C	0.01°C			
XCTD	-2~ 35°C	±0.2°C	0.01°C	0~ 60mS/cm	±0.03mS/c m	0.015mS/c m

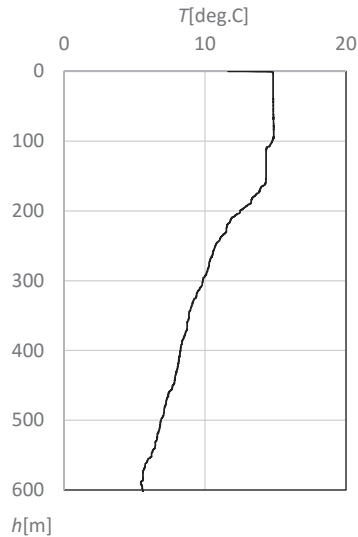


Figure 3.2 Vertical distribution of water temperature

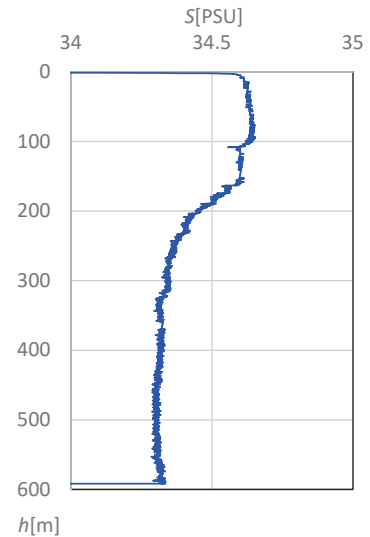


Figure 3.3 Vertical distribution of the salinity

3.3 Measurement of underwater ship radiated noise

The USRN of the target ship was measured by using the hydrophone hanged down from the measurement boat. The target ship ran straight in front of the measurement boat and the noise signal was recorded.

3.3.1 Measurement method

The position of the target ship, measurement boat and the hydrophone is shown in Fig. 3.4, and the test course is shown in Fig. 3.5. Global Positioning System (GPS) are set on both the target ship and the measurement boat. The relative distance between the target ship and the measurement boat are set as 100m, 300m and 500m, although the achieved distance is not strictly followed by these numbers due to drifting of measurement boat.

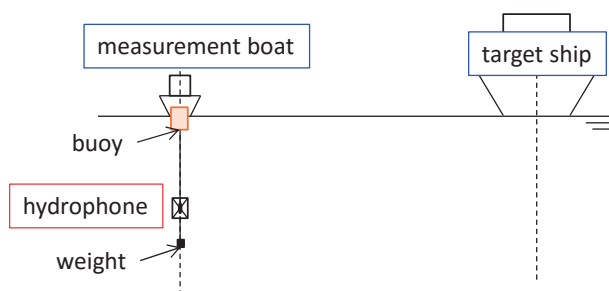


Figure 3.4 Position of the measurement system

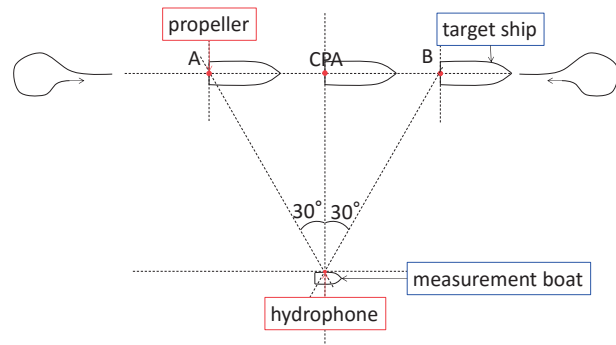


Figure 3.5 Test course

The test conditions are shown in Table 3.2. The engine loads are set as HALF, FULL and NAVI-FULL. As the reference, mean speeds of propeller revolution (revolution per minute, rpm) at the HALF, FULL and NAVI-FULL are 231.7 rpm, 279.3 rpm and 295.9 rpm, respectively. Actual distance between the target ship and measurement boat is obtained from the GPS data. In Table 3.2 “Side” means which broadside the measurement boat is positioned observing from the target ship. The background noise was measured at the position more than 1 nautical mile from the target ship.

Table 3.2 Test condition

Japan standard time	Test number	Engine load	Target distance [m]	CPA * [m]	Side
10:00	-	Back ground noise			
10:18	1	Rehearsal			
10:42	2	HALF	100	105.4	Right
10:54	3	HALF	100	91.4	Right
11:07	4	FULL	100	79.3	Right
11:19	5	FULL	100	111.8	Left
11:30	6	NAVI FULL	100	74.4	Right
11:40	7	NAVI FULL	100	85.8	Left
12:00	8	NAVI FULL	300	219.4	Right
12:11	9	NAVI FULL	300	323.8	Left
12:23	10	NAVI FULL	500	366.1	Right
12:34	11	NAVI FULL	500	510.2	Left
12:59	12	FULL	100	94.4	Right
13:10	13	NAVI FULL	100	129.2	Right
13:21	14	NAVI FULL	100	165.3	Left
13:31	15	NAVI FULL	100	142.5	Left
13:42	16	NAVI FULL	300	332.3	Right
13:54	17	NAVI FULL	500	486.1	Right
14:15	-	Back ground noise			

*: Closet Point of Approach

3.3.2 Measurement device

The device list, the system diagram and the picture of the hydrophone and the buoy are shown in Table 3.3, Fig. 3.6 and Fig. 3.7, respectively.

Table 3.3 Device list

Item	Model number	Number	Maker
Hydrophone	BK8104	1	B&K
Amplifier	Isako 143N	1	Isako
Data recorder	PXI-1031	1	N1
GPS receiver	DGPS212(JLR-4331)	2	JRC/T

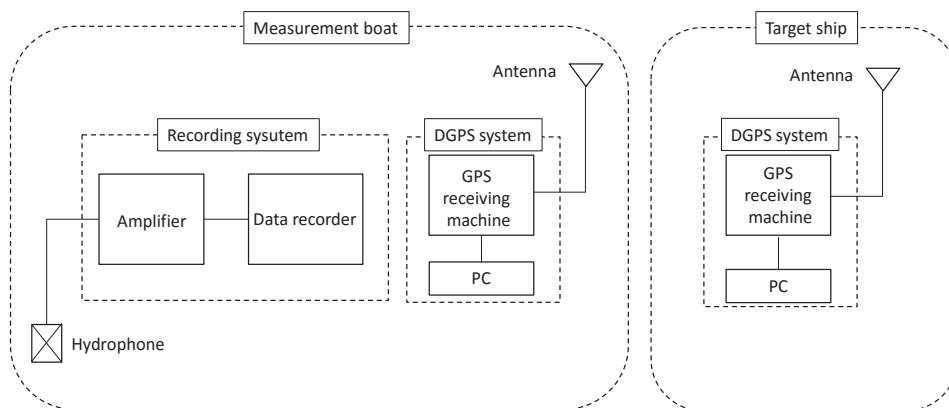


Figure 3.6 System diagram



Figure 3.7 Hydrophone and buoy

3.3.3 Analysis method

Frequency method: The Frequency analysis is carried out using the recorded sound from Point A to Point B shown in Fig. 3.5. The root-mean squared SPL is obtained by the frequency analysis per 1Hz and 1/3 octave band. The sampling frequency at the measurement was 51.2 kHz. High pass filter is applied for which the cut-off frequencies are 10Hz and 20Hz for the data reduction and post-process, respectively.

Distance normalization: The slant range between the target ship and the hydrophone is obtained as:

$$D_T = \sqrt{D_H^2 + D_V^2} \quad (3.1)$$

where D_T is the distance between the shaft center of the target ship and the hydrophone at closest point of approach (CPA) shown in Fig. 3.5, D_H is the horizontal distance and D_V is the vertical distance. The source level L_{pdn} (dB ref. 1 μ Pa) is obtained by Eq. (3.2) and Eq. (3.3) assuming the spherical spreading.

$$L_{pdn} = L_p + 20\log(R) \quad (3.2)$$

$$R = \frac{D_T}{D_0} \quad (3.3)$$

where D_0 is 1 m and L_p is the sound pressure level at the position of the hydrophone.

3.3.4 Results

Figure 3.8 is the comparison in terms of the broadside of the measurement boat, Fig. 3.9 is the comparison in terms of the distance between the target ship and the measurement and Fig. 3.10 is the comparison in terms of the engine load. Among these figures the vertical axis is the source level obtained by Eq. (3.2). In Figs. 3.8 and 3.9 the results are filtered by 1/3 octave band while it is not in Fig. 3.10.

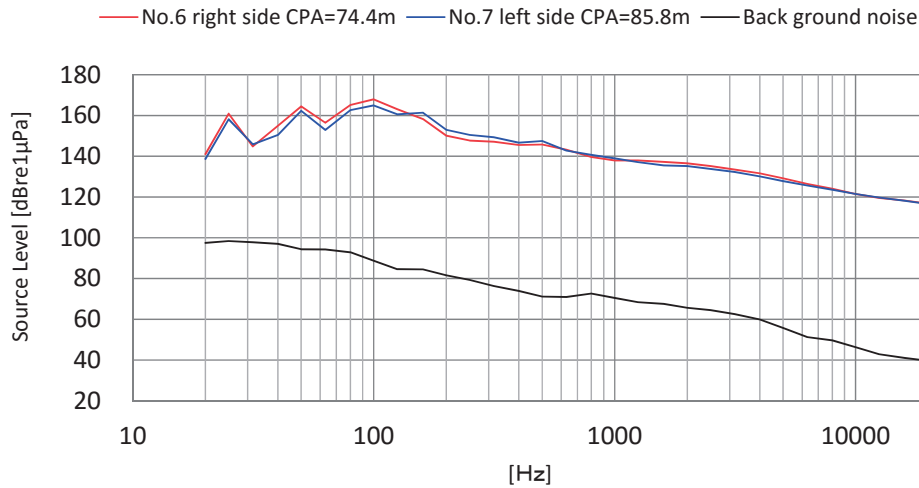


Figure 3.8 Comparison of the source level in terms of the side (Target distance: 100m, Engine load: NAVI-FULL)

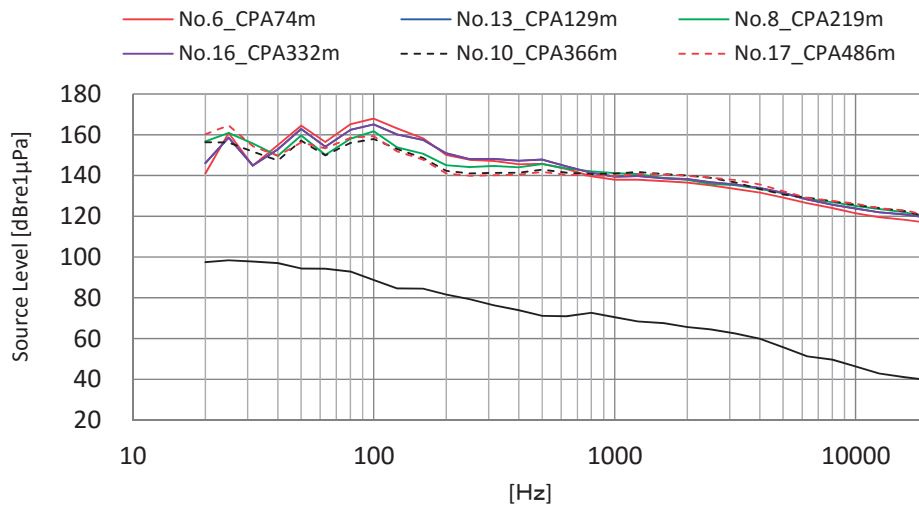


Figure 3.9 Comparison of the source level in terms of the distance (Right side, Engine load: NAVI-FULL)

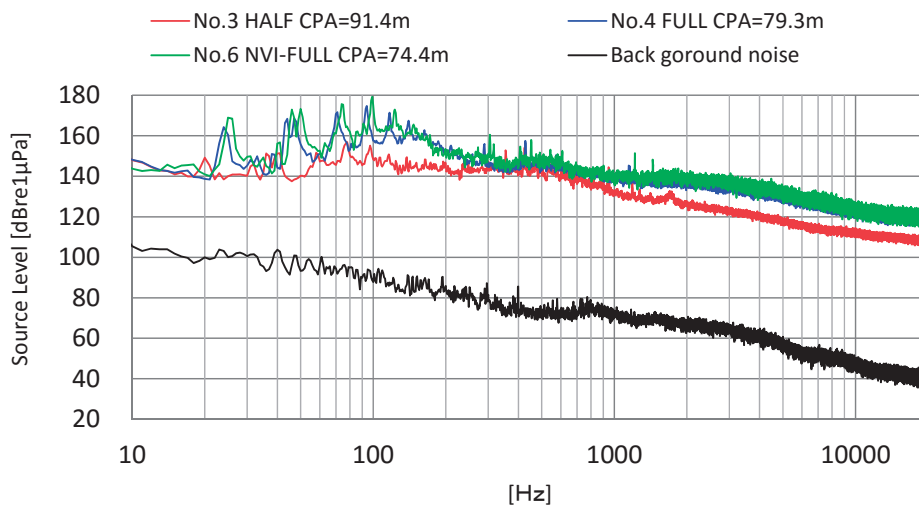


Figure 3.10 Comparison of the source level in terms of the engine load (Right side, Target distance: 100m)

Figure 3.8 shows that the difference due to the broadside is small, but the source level of the right side is slightly higher than that of the left side. This is reasonable since the propeller of the target ship is clockwise rotation observing from the stern. For such propeller, the cavitation extent is more pronounced and remains at starboard side (see for instance, Figs. 2.5 and 2.6 in Chapter 2) than port side, and thus resultant cavitation noise is higher at starboard side than port side. Figure 3.9 indicates that the effect of CPA deviation in the present measurement is small enough and the measured difference in the source level due to engine load is still “meaningful”. Figure 3.10 shows that the source level becomes higher as the engine load successively becomes higher from HALF to FULL to NAVI –FULL. One of the well-known phenomena of USRN is that it has tonal characteristics with blade frequency (BF), i.e. integral multiple of the number of the blade times propeller rotation speed (rps). In the present measurement, the number of the blade is 5 and the propeller rotation speed is 3.9 rps, 4.7 rps and 4.9 rps at HALF, FULL and NAVI-FULL, respectively. In the case of FULL and NAVI-FULL, the frequencies of tonal noise up to 5th order coincide with 5th order of BFs. On the other the tonal noise in the case of HALF is less pronounced than that of FULL and NAVI-FULL. This means that the propeller cavitation and resultant noise are also less apparent than those of FULL and NAVI-FULL.

4. Review of relevant EU projects

4.1 Three EU projects related to ship radiated noise

The 7th Framework Programme (7th FP) of the European Commission funded three European Union (EU) projects related to ship radiated noise, e.g. 1) SILENV (Ship Innovative soLutions to rEduce Noise and Vibrations)³, 2) AQUO (Achieve Quieter Oceans by shipping noise footprint reduction)⁴ and 3) SONIC (Suppression Of underwater Noise Induced by Cavitation)⁵. They are all multinational collaborative projects as summarized in Table 4.1.

Table 4.1 Summary of EU projects

Name(Year)	Work Package	Participants(Nation)
SILENV (2009-2012)	WP0: Management WP1: Noise related needs WP2: Noise measurements WP3: Solutions WP4: Models WP5&6: Green Label requirements	DCNS (France), U.Genoa (Italy), TSI (Spain), SSPA (Sweden), CETENA (Italy), ACCINOVA (Spain), BV (France), CEHIPAR(Spain), HTP-TUV (Bulgaria), INSEAN (Italy), TNO (Netherland), U. Strathclyde/Grasgow (U.K.), VTT (Finland), UPC (Spain)
AQUO (2012-2015)	WP1: Noise footprint assessment model WP2: Noise sources WP3: Noise measurements WP4: Sensitivity on marine life WP5: Guidelines to reduce ship noise footprint	DCNS (France), TSI (Spain), BV (France), UPC (Spain), Quiet-Oceans (France), SSPA (Sweden), U. Genoa (Italy), U. Strathclyde (U.K.), CEHIPAR (Spain), CTO (Poland), IMARES (Netherland), FOI (Sweden), CESA(17 member states from EU countries)
SONIC(2012-2015)	WP1: Accurate cavitation noise predictions WP2: Full scale observations WP3: Noise mapping and mitigation measures WP4: Management WP5: Dissemination	MARIN (Netherland), INSEAN (Italy), HSVA (Germany), Navantia (Spain), Rolls-Royce (U.K.), U. Southampton (U.K.), Wartsila (Italy), TNO (Netherland), ARTTIC (EU multinational), Chalmers U.T. (Sweden), CETENA (Italy), DNV-GL (Germany)

Each project has Work Packages (WP) and they are interconnected one to other as illustrated in Fig. 4.1¹⁸⁾¹⁹⁾.

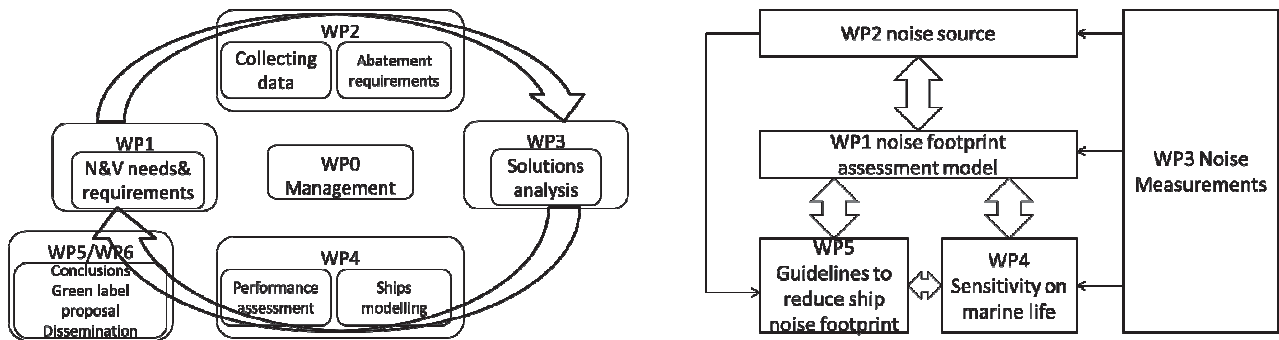


Figure 4.1 WP relationship: (a) SILENV¹⁸⁾, (b) AQUO¹⁹⁾

Simply stated, the characteristics of these projects are;

SILENV : Relatively academic approach for noise and vibration problems inside/outside of the ship

AQUO : Continued project from SILENV. Assessment of ship radiated noise for marine life is added.

SONIC : Arose from AQUO and specifically focuses on propeller cavitation noise

It is noteworthy that all the EU projects have WP for which its task is to establish standards/guidelines for ship radiated noise and their impact on marine fauna, such as clearly stated in the reference¹⁹⁾ as

“... the final goal of AQUO project (Achieve QUIeter Oceans by shipping noise footprint reduction – www.aquo.eu) is to provide policy makers with practical guidelines, acceptable by shipyards and ship owners. The list of solutions will be split into solutions regarding ship design (including propeller and cavitation noise), and solutions related to shipping control and regulation.” (Audoly et al. 2014)¹⁹⁾

4.2 Some representative results from SILENV, AQUO and SONIC

The official deliverables from SILENV are available from its website³⁾ yet the site is somewhat not accessible, and thus the representative result from SILENV is cited from the available references¹⁸⁾. The official deliverables from AQUO and SONIC are mostly able to be obtained from their websites⁴⁾⁵⁾. AQUO and SONIC has also released “Guidelines for Regulation on UW Noise from Commercial Shipping”²⁰⁾ which is downloadable from SONIC website⁵⁾. The representative results from AQUO and SONIC introduced herein are cited from the guidelines²⁰⁾.

4.2.1 SILENV

Especially for marine fauna subjected to the effect of underwater radiated noise (URN), SILENV’s interest is Cetaceans. The upper limit of URN goes “in the direction of a decrease of the diffused background noise of the oceans, responsible mainly for communication masking problems for large marine mammals. “ The underwater noise signatures of different kind of vessels measured in SILENV are utilized to establish the limit curves as shown in Fig. 4.2. Two curves are provided, i.e. one is for design speed (termed “Transit mode”) and the other is for reduced speed (termed “Quiet mode”), yet no distinction is made among different ship types. This is a part of requirements for “Green Label” which is pre-normative limits, e.g. 1) noise and vibrations inside the ship, 2) airborne radiated noise (ARN) and 3) URN, finalized by SILENV.

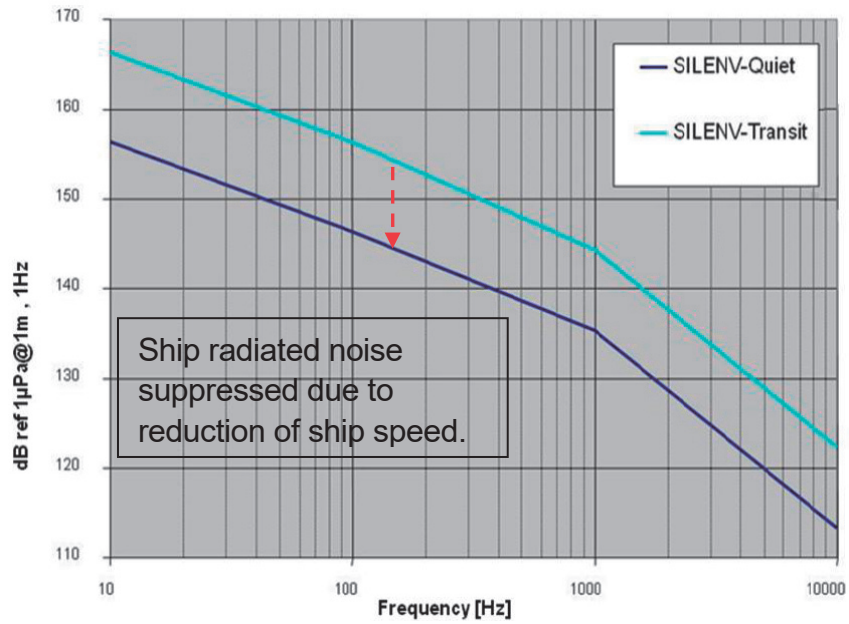


Figure 4.2 URN “Green Label” requirements⁸⁾

4.2.2 AQUO

Different from SILENV, the marine fauna which AQUO is interested in are 1) the Atlantic cod, 2) the harbor porpoise and 3) cuttlefish. The noise limits to 1) and 3) are investigated and reported in the guidelines²⁰⁾ and summarized in Table 4.2.

Table 4.2 SPL limits to marine fauna proposed by AQUO

Frequency (Hz)	SPL* limits for Atlantic cod	SPL* limits for Cuttlefish
63	115	107
125	131	119

*: dB re.1µPa²

These limits are utilized to illustrate the assessment of masking spawning communication and potential behavioral reaction to shipping noise. Figure 4.3 is its example for Atlantic Cod.

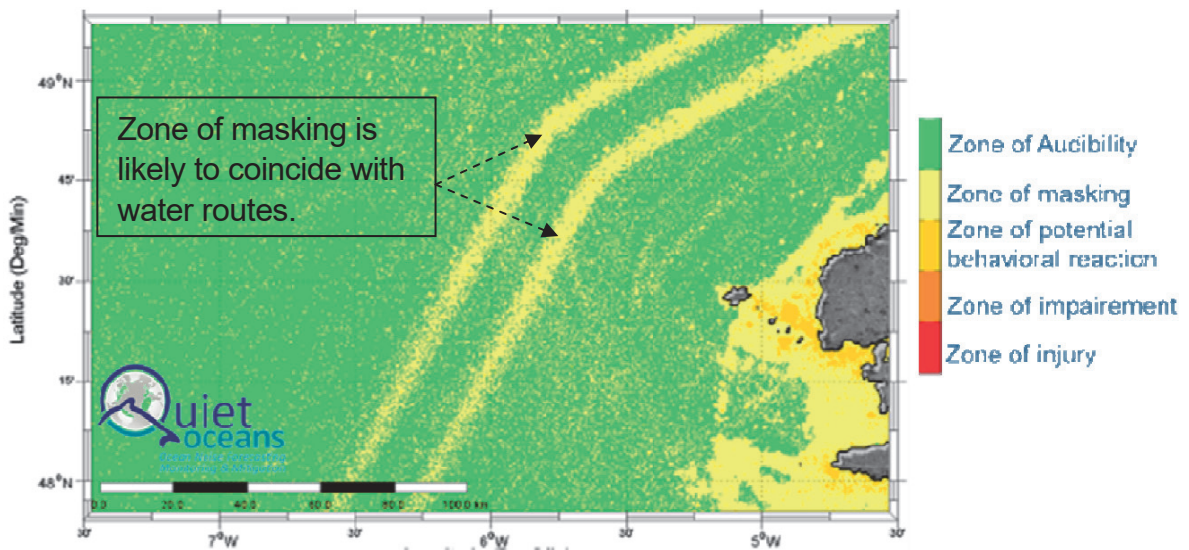


Figure 4.3 Illustration of assessment of masking spawning communication and potential behavioral reaction to shipping noise in June 2014 for Atlantic Cod offshore Brest²⁰⁾

AQUO also suggests parametric composite-spectrum URN model which is basically a linear summation of machinery noise, propeller noise (non-cavitating) and propeller cavitation noise as shown in Equation (4-1)²⁰.

$$SL_{V3E}(f, V, L_{ref}) = 10 \log \left(10^{\frac{SL_{mach-improved}(f, V, L_{ref})}{10}} + 10^{\frac{SL_{prop-improved}(f, V, L_{ref})}{10}} + 10^{\frac{SL_{cav-improved}(f, V, L_{ref})}{10}} \right) + LF_{corr}(f, d) \tag{4-1}$$

where $LF_{corr}(f, d)$ is the Lloyd Mirror effect correction given by

$$LF(f, d) = \text{Max} \left[0; \log \left(\frac{1}{2} + \frac{1}{(2(2\pi f/c)d(L)\sin\theta)^2} \right) \right], d = \text{source depth}, \theta = 15 \text{ deg.} \tag{4-2}$$

In Eqs. (4-1) and (4-2), SL_{V3E} is the total source level (dB re. $1\mu\text{Pa}^2/\text{Hz}@1\text{m}$), f is the target frequency, V is the vessel speed, L_{ref} is the vessel size with respect to a reference length for ships' category, $SL_{mach-improved}$ is the noise radiated by internal machinery and equipment, transmitted to water through the hull, $SL_{prop-improved}$ is the noise radiated by the non-cavitating propeller, and $SL_{cav-improved}$ is the noise radiated by the cavitating propeller. There are 14 model constants in the first term of log bracket in Eq. (4-1)¹⁹ which are to be identified by regression analysis using database such as "Ship Underwater Radiated Noise Database: <http://vesselnoise.soton.ac.uk/>". Figure 4.4 shows the example of source level estimated by the AQUO's parametric composite-spectrum URN model.

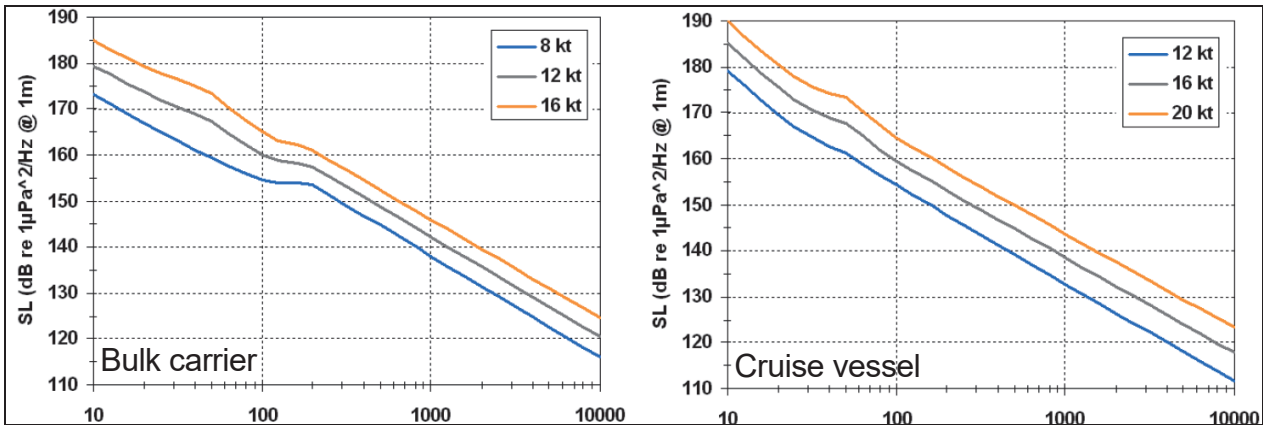


Figure 4.4 SL estimated by the AQUO's parametric URN model²⁰, 180m bulker (left) and 250m cruise vessel (right)

AQUO proposes measurement standard for URN which is applicable to both deep and shallow water environment²⁰ and Bureau Veritas has recently released voluntary notation "NR614" about URN measurement²¹ in accordance with the outcome from AQUO as summarized in Table 4.3.

Table 4.3 Overview of “NR614” measurement procedure²¹⁾

Type of waters	Shallow	Deep
General		
Assumption	Ship considered as a monopole source	
Resulting quantity	Underwater noise signature of the ship expressed in terms of spectral density of the sound pressure level (in dB, ref 1µPa@1m/Hz).	
Measurement Uncertainty	±4dB (±5.5dB if only two 2 runs are performed)	±3.5dB (±5dB if only two runs are performed)
Frequency range	10Hz-50KHz (1/3 octave band)	
Test site requirements		
Minimum sea depth	Max (60m, 0.3v ²)	Max (200m, 2 x ship length)
Weather conditions	≤ Beaufort 3	≤ Beaufort 2
Sea bottom	Flat and homogeneous, without slope or seabed features	
Noise recording		
Configuration	Bottom mounted	Floating or bottom mounted
Number of hydrophones	3	
Hydrophone deployment		
Distance measurement		
Maximum uncertainty	+/-10m	
Tilt angle	It shall be measured if no direct distance measurement is carried out.	
Complementary measurements		
Vessel speed	Required	
Celerity profile measurements	If numerical TL is used, measurements with a CTD or a direct sound speed sensor have to be carried out every 2m.	
Measurement test sequence		
Nominal distance to CPA	Max(200m, 1 x ship length) or max (100m, 1xship length) if significant background noise	
Number of runs	6 runs (2 runs if GT > 10000)	
Test course configuration		
Post-processing		
Recorded signal split into several data windows		
Data window		
Post processing main steps	<ul style="list-style-type: none"> • SPL spectrum calculation on each data window • Background noise correction • Distance correction (using numerical modelling) • Power average on all hydrophone • Linear average on all data windows • Linear average on all runs 	

4.2.3 SONIC

One of the important outcomes from SONIC is the footprint and mapping of URN. The aims of developing these tools are²⁰⁾:

- Assessing design guidelines intended to minimize the noise footprint of a specified ship design
- Visualizing the total noise from shipping activity in a specified area
- Producing noise maps suitable for the European Atlas of the Sea
- Assessing effect on noise maps of spatial planning of ship traffic

Figure 4.5 is the example of shipping noise map²⁰⁾. It is generated using ship distribution (i.e. AIS data), animal hearing sensitivity and animal depth distribution (target animal is harbor porpoise for this example).

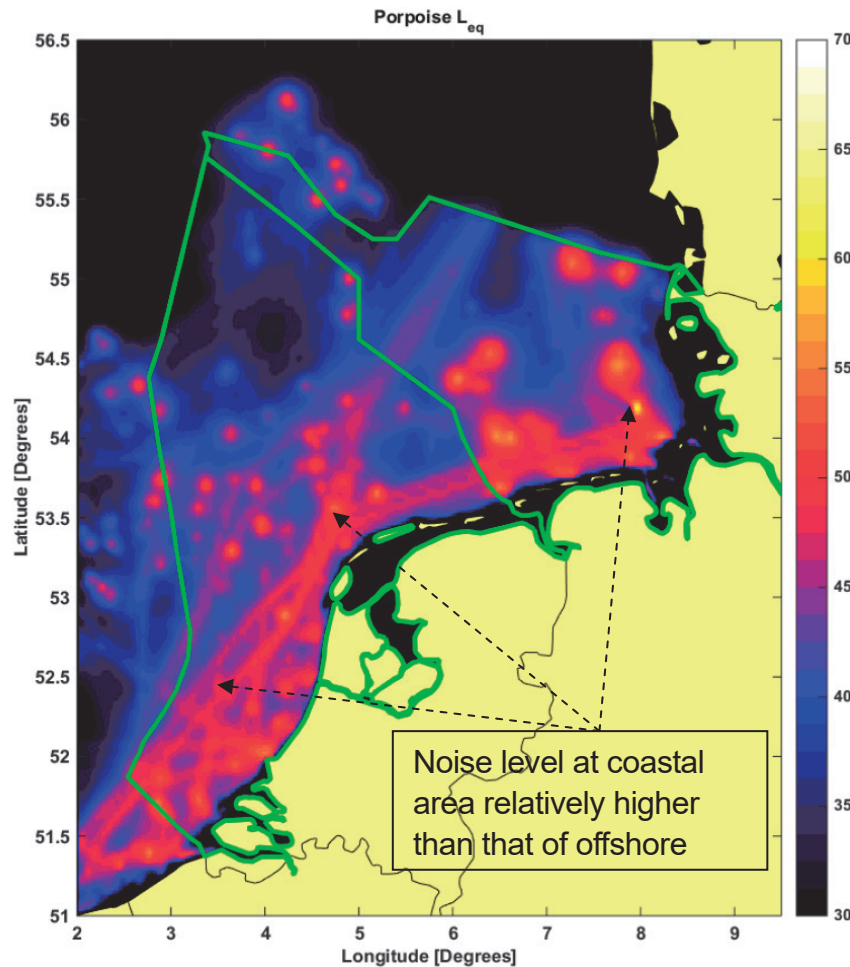


Figure 4.5 Annual average shipping noise map for harbor porpoise in Dutch and German waters²⁰⁾

5. Concluding remarks

Exploratory studies are carried out to investigate computational and measurement methods for USRN. For computational estimation of near field propeller cavitation noise, viscous CFD is able to predict sheet cavitation pattern accurately as well as to quantify cavitation extent. The former result in the accurate estimation in tonal noise by direct estimation, and the latter contributes to predict upper bound of broadband noise together with the Brown's formula. For field measurement of USRN carried out at Nishiizu waters of Japan, variations of the source level due to difference in broadside and engine load are well captured and the data would be quite useful for future validations for computational results. Reviews of state-of-art EU projects manifest the current guidelines for underwater ship radiated noise suggested by SILENV, AQUO and SONIC and

their technical backgrounds. In consequence, the results from present exploratory study are encouraging in that 1) the validity and availability of viscous CFD are shown for near field propeller cavitation noise, 2) the current measurement procedure is valid to estimate source level of USRN originated from cavitating propeller, and 3) state-of-arts are understood for three EU projects relevant to USRN. They give indications to the on-going domestic projects for their future tasks.

Acknowledgements

Part of this research was funded by the Ocean Development and Environment Policy Division in Maritime Bureau at Ministry of Land, Infrastructure, Transport and Tourism in Japan, and Japan Ship Technology Research Association with a financial support by the Nippon Foundation.

Reference

- 1) Mitsun R.B. Ed., 1995, Underwater noise of research vessels review and recommendations, International Council for the Exploration of the Sea (ICES), Palaegade 2-4, DK-1261, Copenhagen K, Denmark.
- 2) International Maritime Organization (IMO), 2014, Guidelines for the reduction of underwater noise from commercial shipping to address adverse impact on marine life, MEPC.1/Circ.833.
- 3) Ships oriented Innovative soLutions to rEduce Noise and Vibrations (SILENV), <http://www.silenv.eu/>
- 4) Achieve QUIeter Oceans by shipping noise footprint reduction (AQUO), <http://www.aquo.eu/>
- 5) Suppression Of underwater Noise Induced by Cavitation (SONIC), <http://www.sonic-project.eu/>
- 6) Kamiirisa H. and Goto H., 2005, Development of prediction method for ship underwater noise by bubble dynamics, Mitsui Zosen Technical Review No.185, pp.38-44. (in-Japanese)
- 7) Brown N.A., 1976, Cavitation noise problems and solutions, Proc. International Symposium on Shipboard Acoustics, pp. 21-38.
- 8) STAR-CCM+® Documentation Version 10.06, CD-adapco™.
- 9) Schnerr G.H. and Sauer J., 2001, Physical and numerical modeling of unsteady cavitation dynamics, Proc. 4th International Conference of Multiphase Flow.
- 10) Kato H., Ed., 1999, Cavitation –Fundamentals and state-of-art-, Maki Syoten, ISBN 4-8375-0658-5. (in-Japanese)
- 11) Final Report of SR183, No. 358. (in-Japanese, <http://www.jstra.jp/html/PDF/SR183-5803.pdf>)
- 12) Kurobe Y., Ukon Y., Koyama K and Makino M., 1983, Measurement of cavity volume and pressure fluctuations on a model of the training ship “Seiun-maru” with reference to full scale measurement, Ship Research Institute Technical Review, Vol. 20, No. 6, pp. 395-429. (in-Japanese)
- 13) Kudo T., Ukon Y., Kurobe Y. and Tanibayashi H., 1989, Measurement of shape of cavity on a model propeller blade, Journal of the Society of Naval Architects of Japan, Vol. 166, pp. 93-103. (in-Japanese)
- 14) Bijlard M., 2014, RANS simulations of cavitating azimuthing thrusters, Proc. STAR Global Conference 2014.
- 15) Hasuike N., Yamazaki S. and Ando J., 2010, Numerical simulation of propeller cavitation including tip vortex resolution, Journal of the Japan Society of Naval Architects and Ocean Engineers, Vol. 11, pp. 29-40. (in-Japanese)
- 16) Kanemaru T. and Ando J., 2011, Numerical analysis of pressure fluctuation on ship stern induced by cavitating propeller using a simple surface panel method “SQCM”, Proc. 2nd International Symposium on Marine Propulsors (SMP’11), Hamburg, Germany.
- 17) Hoshino T., Jung J., Kim J.H., Lee J.H., Han J.M. and Park H.G., 2010, Full scale cavitation observations and pressure fluctuation measurements by high-speed camera system and correlation with model test, Proc. International Propeller Symposium (IPS) 2010, Okayama, Japan.
- 18) Badino A., Borelli D., Gaggero T, Rizzuto E. and Schnone C., 2013, The EU research effort towards the control of noise emission from ships: the SILENV Project (7FP), Proc. AIA-DAGA 2013 Conference on Acoustics, pp.963-966.

- 19) Audoly C., Rousset C., Folegot T., Andre M., Benedetti L. and Baudin E., 2014, AQUO European collaborative project-Development of methods and indicators for the assessment of shipping noise footprint on underwater environment and impact on marine life, Transport Research Arena 2014, Paris, France.
- 20) Bureau Veritas and DNV GL Ed., 2015, Guidelines for regulation on UW noise from commercial shipping (Revision 4.3), Achieve Quieter Oceans by shipping noise footprint reduction, FP7-Grant agreement No. 314227/Suppression of UW noise induced by cavitation, FP7-Grand agreement No.314394.
- 21) Palomo P.B., Mullor R.S. and Rodriguez A.M., 2015, A comprehensive framework to address ship underwater radiated noise: From Bureau Veritas class notation to validations of numerical prediction tools, Proc. 22nd International Congress on Sound and Vibration, Florence, Italy.